The Journal of Chemical Physics

Laser-based spectroscopy of FeD: Excitations to the g $^6\Phi$ electronic state

Cite as: J. Chem. Phys. **158**, 024305 (2023); https://doi.org/10.1063/5.0129919
Submitted: 07 October 2022 • Accepted: 07 December 2022 • Published Online: 11 January 2023

R. A. R. Harvey, D. W. Tokaryk and A. G. Adam

AIP Publishing

The Journal of Chemical Physics ARTICLE scitation.org/journal/jcp

Laser-based spectroscopy of FeD: Excitations to the g $^6\Phi$ electronic state

Cite as: J. Chem. Phys. 158, 024305 (2023); doi: 10.1063/5.0129919
Submitted: 7 October 2022 • Accepted: 7 December 2022 •
Published Online: 11 January 2023

R. A. R. Harvey,[1] D. W. Tokaryk,[1,a)] and A. G. Adam[2]

AFFILIATIONS

[1] Department of Physics, University of New Brunswick, Fredericton, New Brunswick E3B 5A3, Canada
[2] Department of Chemistry, University of New Brunswick, Fredericton, New Brunswick E3B 5A3, Canada

[a)] **Author to whom correspondence should be addressed:** dtokaryk@unb.ca

ABSTRACT

Bands of the g $^6\Phi$-X $^4\Delta$, g $^6\Phi$-A $^4\Pi$, g $^6\Phi$-a $^6\Delta$, and g $^6\Phi$-b $^6\Pi$ electronic transitions of iron monodeuteride (FeD) have been measured in laser excitation and in dispersed fluorescence. The molecules were produced both in a cold supersonic molecular jet source and in a chemical reaction between iron pentacarbonyl [$Fe(CO_5)$] and a microwave discharge of argon and hydrogen gases. Dispersed fluorescence from the latter source was detected at high resolution with a Fourier transform spectrometer, yielding a large number of the transitions observed. The data reveal that FeD experiences strong interstate couplings that compromise fitting of the data with traditional Hamiltonians but that the problem is less severe than in corresponding spectra of FeH. This work greatly expands the available data on FeD, which were previously characterized only through the F $^4\Delta$-X $^4\Delta$ spectrum and pure rotational data in the ground state.

I. INTRODUCTION

Iron hydride, FeH, was first observed when its electronic transitions were identified in solar spectra, especially spectra taken from sunspots, in 1972.[1] It was subsequently identified in S stars and M dwarf stars.[2–4] It gained interest astronomically due to the high abundance of hydrogen and iron in the galaxy, being the first and sixth most abundant elements. Furthermore, FeH was discovered to have a high response to external magnetic fields,[5,6] opening up an avenue for measuring the fields in stellar atmospheres. Analysis of early laboratory experiments[7] confirmed the existence of FeH on sunspots, but the complexity of the spectrum precluded rotational assignments of the data. In fact, no rotational analysis was achieved until 1983 when Balfour *et al.*[8,9] were able to characterize the F $^4\Delta$–X $^4\Delta$ transition in the isotopologue FeD as the substitution of deuterium simplified the spectrum. With these results in place, Phillips *et al.*[10] were finally able to analyze the same transition in FeH in 1987.

A seminal theoretical study in 1990[11] on the electronic structure of FeH provided a framework for further laboratory studies, and it was followed by a study in 2012[12] that focused on the X $^4\Delta$, A $^4\Pi$, a $^6\Delta$, and b $^6\Pi$ states. Between 1990 and 2009, Brown's group greatly extended the experimental characterization of FeH by identifying transitions involving the a $^6\Delta$, b $^6\Pi$, c $^6\Sigma^+$, e $^6\Pi$, and g $^6\Phi$ electronic states in the sextet manifold[13–20] and transitions involving the A $^4\Pi$, C $^4\Phi$, and E $^4\Pi$ states in the quartet manifold.[18,21,22] They also performed laser magnetic resonance experiments to measure far-infrared pure rotational transitions in a number of spin–orbit components of the X $^4\Delta$ ground state of FeH.[23] At the completion of these studies, the electronic structure of FeH was well established.

However, other than Balfour's F $^4\Delta$–X $^4\Delta$ transition reported in 1983,[8,9] an infrared matrix isolation study of FeH and FeD trapped in argon,[24] and laser magnetic resonance experiments on the ground state reported by Brown's group in 2009,[25] no spectroscopy has been performed on the FeD isotopologue of iron hydride. In this paper, we report on electronic transitions in FeD that arise from pumping levels in the g $^6\Phi$ state with a tunable laser. The transitions observed were g $^6\Phi$–X $^4\Delta$, g $^6\Phi$–a $^6\Delta$, g $^6\Phi$–b $^6\Pi$, and g $^6\Phi$–A $^4\Pi_{5/2}$ (v = 1). Figure 1 schematically illustrates the various vibrational and spin–orbit levels involved. The data were obtained in two different sources with laser excitation spectroscopy and dispersed fluorescence spectroscopy. As a result of this work, the experimental characterization of FeD has been greatly extended.

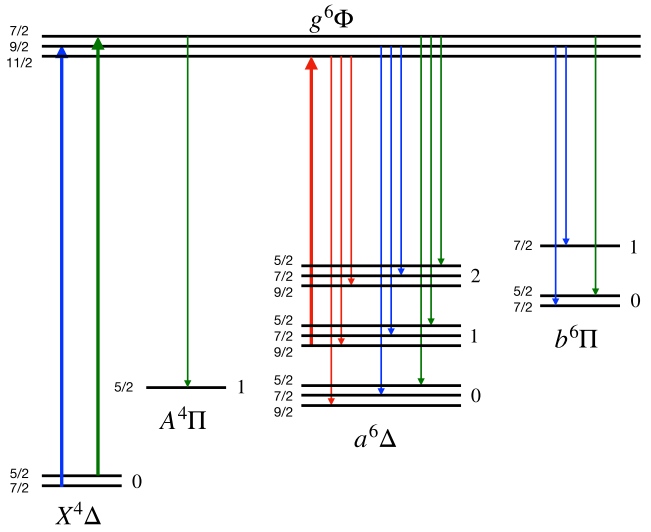

FIG. 1. Schematic summary of the transitions involved in this study of FeD (states not involved in this work are not shown). Each state is represented by a horizontal line, with the electronic label given above or below each stack of lines. The value of Ω, the projection of total angular momentum J along the internuclear axis of the molecule for a given spin-orbit substate, is given on the left and the vibration on the right. Transitions excited with a laser are shown as thicker vertical arrows pointing upward, and those observed in dispersed fluorescence as thinner vertical arrows pointing downward. Groupings of connected levels described in Sec. IV A are given in different colors.

II. EXPERIMENTAL

A. Production of FeH and FeD

We produced FeH and FeD for study in two different sources: a pulsed molecular jet source and a continuous source based on the design of Beaton *et al.*[26] as implemented in John Brown's group.[14] Our initial experiments were conducted on FeH in the laser ablation molecular jet source at the University of New Brunswick,[27] with an iron rod installed in the vacuum chamber and various hydrogen-bearing precursors mixed in a plenum with helium. Gas from the plenum was regulated to 40 psi before it was admitted into the vacuum chamber. The rod was ablated with 10 ns pulses of 355 nm laser light produced by a Lumonics HY400 Nd:YAG laser, with a pulse of gas from the plenum timed for release in concert with the ablation pulse. Reactions between the ablated iron atoms and precursor gases were expected to form FeH. Low-resolution survey scans were conducted with light from a Lumonics HD500 pulsed dye laser pumped with a Lumonics YM600 Nd:YAG laser. C450 laser dye was used to access wavelengths in the g $^6\Phi$–X $^4\Delta$ spectrum. The linewidth of isolated spectral lines taken with the pulsed system was about 0.5 cm^{-1}.

While we succeeded in producing FeH in the laser ablation source, the signal was noisy and inconsistent from scan to scan. We next adapted the technique of Beaton *et al.* for use in the jet apparatus. In this case, the plenum was filled with 150 psi of helium, 5 psi of hydrogen, and vapor from the volatile liquid iron pentacarbonyl [$Fe(CO)_5$] added to the limit of its vapor pressure at room temperature, about 20 Torr. This mixture was regulated to 40 psi, then admitted into the molecular jet apparatus, with the ablation laser blocked and a pair of annular electrodes added at the point where the gas pulse entered the high-vacuum region. A pulsed potential difference of about 3000 V applied across the plates produced a strong discharge when timed to coincide with the passage of a gas pulse from the plenum through the plates. When the jet emerging from the discharge region was probed as described above with the pulsed dye laser beam, a much stronger spectrum of FeH was obtained. A comparison of the ablation and discharge jet spectra is shown in Fig. 2. From the distribution of intensity among rotational levels within a band, we estimate that the equivalent temperature of molecules in the jet source is about 50 K.

We also produced FeH and FeD in a continuous rather than a pulsed manner by adapting a Broida oven body formed from a six-way cross vacuum chamber to John Brown's procedure. A flowing mixture of argon (~1.8 Torr) and hydrogen or deuterium (30–50 mTorr) was admitted into one arm of the Broida chamber through a 1/2 in. quartz tube. The gases were discharged in an Evenson cavity with microwaves supplied at 75 W by a Microtron 200 generator. A Teflon liner inside the tube just past the discharge zone greatly slowed the recombination of atomic hydrogen or deuterium. A length of 1/8 in. steel tubing entering from the bottom of the vacuum chamber admitted 5–10 mTorr of $Fe(CO)_5$ vapor just at the mouth of the quartz tube. The reaction between the $Fe(CO)_5$ and the discharge products produced a horizontal streak of green fluorescence from atomic iron. When the streak was probed by a blue cw laser beam, introduced from the top of the Broida chamber via an optical fiber, laser-induced fluorescence could be observed by eye when the beam frequency was tuned to resonance in FeH. We will refer to the continuous source as the room-temperature source (RT source) hereafter, to distinguish it from the low-temperature discharge jet source described above. Figure 3 shows picture of the interior of the RT source while in operation.

B. Experiments performed on FeD

FeD molecules were probed either by the pulsed dye laser system described above or with radiation from a cw Coherent 699-21 ring dye laser run with Stilbene 420 dye, pumped with all UV lines from an argon ion laser. Both laser excitation and dispersed fluorescence spectroscopies were performed.

For laser excitation scans taken from the molecular jet source, the pulsed (~2 mJ/pulse) or cw (~200 mW) laser beam passed about 5 cm below the orifice admitting the gas pulse into the chamber. Laser-induced fluorescence passed through a slitless monochromator of 0.25 m focal length to limit the bandwidth to about a 30 nm window and was detected with a thermoelectrically cooled Hamamatsu R943-02 phototube. The signal was processed with either a boxcar integrator or a Stanford Research Systems SR400 photon counter. Linewidths from the molecular jet source were typically about 200 MHz (~0.007 cm^{-1}) for spectra taken with the cw ring laser. To calibrate the laser excitation scans, fringes from a thermally stabilized 300 MHz plane-mirror etalon and optogalvanic spectra of a uranium/argon hollow cathode lamp were recorded along with the signals from FeD. We estimate that the uncertainty in the absolute frequencies of well-resolved single lines is about 0.002 cm^{-1}.

Radiative lifetimes were obtained from a number of rotational levels in the g $^6\Phi_{9/2}$ and g $^6\Phi_{7/2}$ states in the jet source, which provides an essentially collision-free environment. The measurements were made by displaying the time evolution of the laser-induced fluorescence recorded by the phototube on a Tektronix TDS430

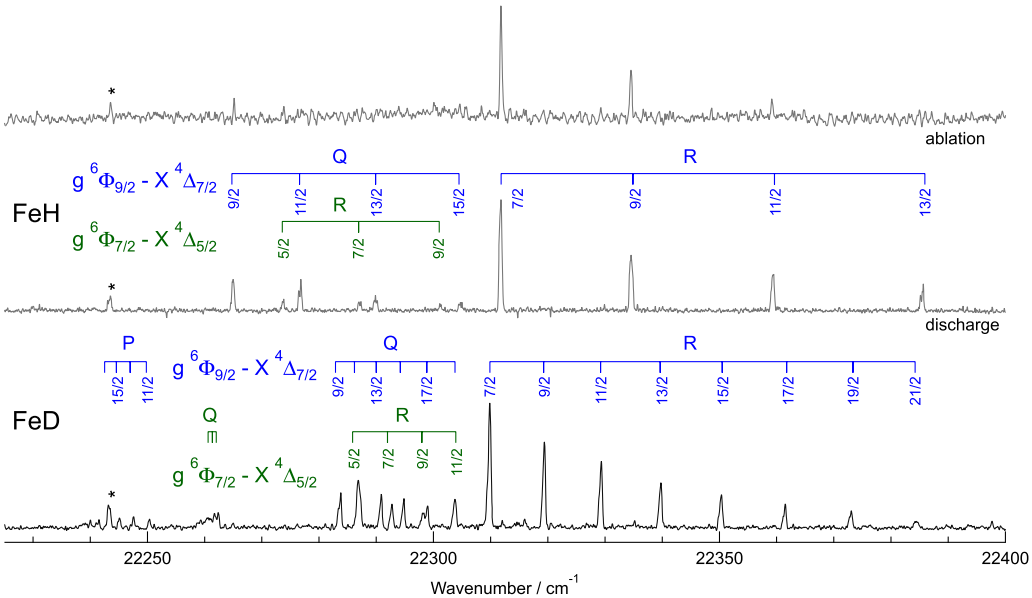

FIG. 2. Spectra of FeH and FeD obtained with pulsed-laser excitation spectroscopy from the UNB molecular jet source. The top trace was obtained by ablating an iron rod in the presence of a gas pulse containing B_2H_6 to produce FeH. In the middle trace, FeH is produced via the jet discharge technique described in the text, using a mix of helium, $Fe(CO)_5$, and hydrogen gas. The bottom trace shows the spectrum of FeD obtained with the discharge technique, substituting deuterium for hydrogen. In the lower two traces, branches of the g $^6\Phi_{9/2}$–X $^4\Delta_{7/2}$ transition are drawn in blue, and those of the g $^6\Phi_{7/2}$–X $^4\Delta_{5/2}$ transition are shown in green. The line marked with an asterisk is due to atomic iron.

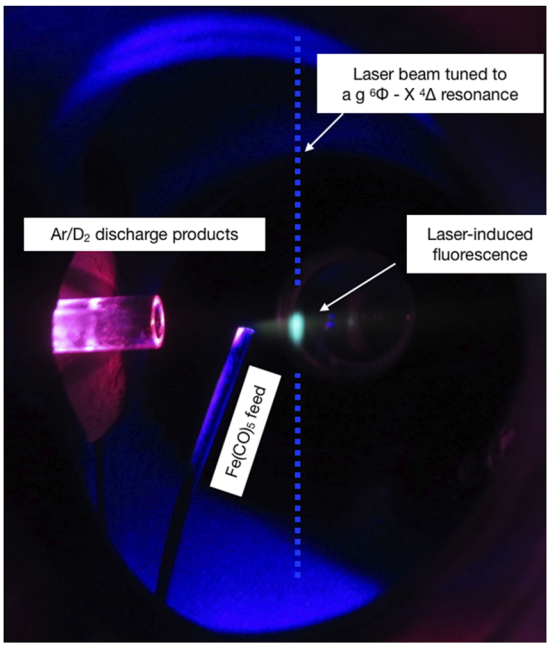

FIG. 3. The interior of our FeD source, based on the source used in Brown's group,[26] under operating conditions. The horizontal green streak described in the text is less prominent here than it can be. Note the green fluorescence arising from the g $^6\Phi$–a $^6\Delta$ transition when the laser is tuned to a resonance of the FeD g $^6\Phi$–X $^4\Delta$ transition in the blue. The Teflon liner is not visible but can be extended to the end of the quartz tube if desired.

oscilloscope (400 MHz bandwidth), which was set to perform a running average of 1024 traces. The input impedance of the oscilloscope was set to 50 Ω. The averaged trace was saved as a digital file for processing. Tests performed in our source with this technique using atomic transitions with known lifetimes indicate that we can accurately measure lifetimes less than about 200 ns with helium as a carrier gas and 900 ns with argon; longer-lived states can move out of our viewing window before fluorescing and the measured lifetimes are artificially shortened as a result.

For use in the RT source, the laser beam was directed into a multimode optical fiber that delivered 100–150 mW of power from the ring dye laser to the experiment. The laser-induced fluorescence was then directed into a Spex 1700 grating spectrometer with a 0.75 m focal length, which provided a variable bandpass of 2–100 cm^{-1} depending on the width set on its slits. A cooled RCA 31034A phototube detected the light coming from the spectrometer, and a Keithley 414A picoammeter measured the resulting photocurrent. Linewidths from the RT source were typically 0.038 cm^{-1} in the blue-green spectral region, limited by the room-temperature Doppler broadening of FeD.

Dispersed fluorescence spectra were collected from the RT source with a Bomem DA3.002 Fourier transform spectrometer run as described in Ref. 28. A Thorlabs FESH0600 shortpass filter was used to limit the observed wavelengths to 400–600 nm, thereby strongly suppressing scattered light from the spectrometer's helium–neon reference laser. The interferograms were collected with a Hamamatsu R-928 photomultiplier tube. The input iris was set typically to a diameter of 1–1.5 mm, which limited the linewidths of well-resolved features to 0.08–0.12 cm^{-1}. Around 50–70 interferograms were coadded and transformed to produce the final spectra.

Calibration of the Fourier transform spectra was achieved using both lines of atomic iron[29] from the green background fluorescence in the source as well as with FeD lines already measured in laser excitation. Some of the data were taken in air rather than in vacuum, in which case calibration was performed with air wavenumbers, with the air wavenumber of measured features corrected back to vacuum values afterward. The absolute uncertainty in the Fourier transform peaks is estimated to be 0.007–0.010 cm^{-1}, based on the widths of the lines and on statistical analysis of peaks measured multiple times in different spectra.

III. DATA

A. Laser excitation spectra of the g $^6\Phi$–X $^4\Delta$ transition

The g $^6\Phi$–X $^4\Delta$ transition was studied via laser excitation spectroscopy in the discharge molecular jet source. As discussed in Ref. 14, while the g $^6\Phi$ state is accessible from the X $^4\Delta$ state using laser light at ~448 nm, the g $^6\Phi$ state fluoresces most strongly to the a $^6\Delta$ state, resulting in fluorescence near 490 nm (Fig. 3). We therefore detected signal with the slitless monochromator set to 490 nm, which eliminated scattered light from the excitation laser. Once the spectra of the g $^6\Phi$–X $^4\Delta$ transition of FeH were optimized at pulsed resolution using the discharge jet source, a pulsed-resolution survey of the analogous spectrum in FeD was conducted. We found the FeD band in close proximity to that of FeH (see Fig. 2). The spectra were readily assigned with the aid of lower-state combination differences[9,25] to the g $^6\Phi_{9/2}$–X $^4\Delta_{7/2}$ and g $^6\Phi_{7/2}$–X $^4\Delta_{5/2}$ spin–orbit components of the 0-0 band. The intensity distribution was similar to that of FeH, with a strong R branch, moderate Q branch, and weak P branch. We then took short high-resolution laser excitation scans over the observed features using the cw ring laser. A sample scan of the R(9/2) line in the g $^6\Phi_{9/2}$–X $^4\Delta_{7/2}$ band is shown in panel (a) of Fig. 4. Note that the resolution and signal-to-noise ratio are sufficient to identify and resolve the analogous line for the ^{54}FeD isotopologue, which has a natural abundance of 5.8% in our sample as compared to the 91.8% abundance of the dominant ^{56}FeD isotopologue. Parity doubling was observed in a number of transitions, as illustrated in panel (b) of Fig. 4. Combination differences and comparisons with data from Ref. 25 showed that the doubling was attributable solely to the X $^4\Delta$ state in both bands. At this stage, we cannot conclusively determine the parity or $e-f$ labeling of the rotational levels, but following Brown *et al.*[25] we presume that the f levels lie above the e levels in FeD, as they do in FeH. This supposition is subject to future verification. The complete listing of rotational assignments for our g $^6\Phi$–X $^4\Delta$ data is given in Table I.

Although the cooling effect of the molecular jet strongly compresses the rotational, vibrational, and electronic population of the ensemble of molecules to very low-lying states, at times we can see signals from higher-lying metastable states. We succeeded in observing a few lines of the FeH g $^6\Phi$–a $^6\Delta$ 0–0 transition near 490 nm with our pulsed laser due to the metastability of the a $^6\Delta$ state, found about 1900 cm^{-1} above the ground state X $^4\Delta$. When we substituted deuterium for hydrogen in the discharge, the FeH lines disappeared and a few new weak features appeared in their place. These lines were later shown to belong to the 0–0 g $^6\Phi_{11/2}$–a $^6\Delta_{9/2}$ system of FeD when they were obtained with a much higher signal-to-noise ratio using dispersed fluorescence. These observations show that the metastable a $^6\Delta$ state is indeed weakly populated in the molecular jet, presumably facilitated to a degree by the excitation produced by the electrical discharge.

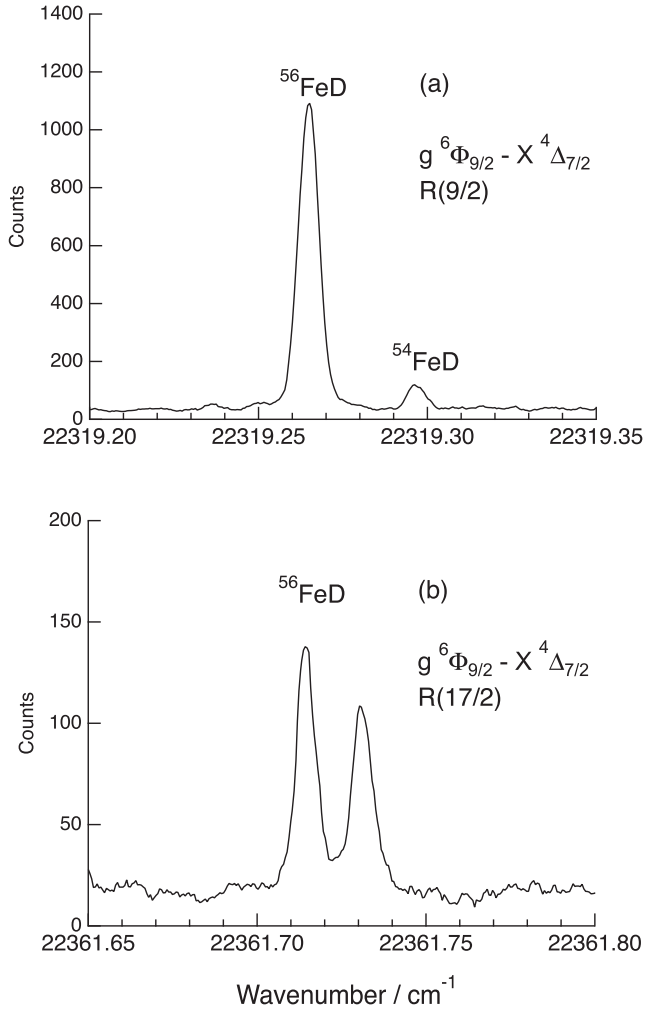

FIG. 4. High-resolution spectra of FeD in our molecular jet source, taken with the ring dye laser. Panel (a) shows the g $^6\Phi_{9/2}$–X $^4\Delta_{7/2}$ R(9/2) line for both the lower-abundance ^{54}FeD isotopologue and the dominant ^{56}FeD isotopologue. Panel (b) shows parity doubling in the R(17/2) line of the same band, for which the ^{54}FeD isotopologue was not observed due to the overall lower intensity of the spectrum.

B. Dispersed fluorescence spectra from the Ω = 9/2 and 7/2 spin–orbit components of the g $^6\Phi$ state

Dispersed fluorescence spectra were recorded from the RT source with the Bomem Fourier transform spectrometer by exciting seven rotational levels in the g $^6\Phi$ state: the J = 9/2, 11/2, and 13/2 levels of the g $^6\Phi_{9/2}$ state through R lines in the g $^6\Phi_{9/2}$–X $^4\Delta_{7/2}$ band and the J = 7/2, 9/2, 11/2, and 13/2 levels of the g $^6\Phi_{7/2}$ state through R lines in the g $^6\Phi_{7/2}$–X $^4\Delta_{5/2}$ band. Figure 5 shows a sample spectrum taken by exciting the J = 11/2 level of the g $^6\Phi_{9/2}$ state; since the parity doubling is not resolved in the R(9/2) line, both parities were excited. The positions of the 0–0 bands of FeD are not

TABLE I. Assigned lines of the g $^6\Phi$–X $^4\Delta$ transition of ^{56}FeD in cm^{-1}, measured in the molecular jet source with a ring dye laser. The absolute uncertainty in the measurements is estimated at 0.002 cm^{-1}. Assignment of *e*/*f* labels assumes that the ordering of these levels in the X $^4\Delta$ state for a given *J* are the same as in FeH. Transitions of ^{54}FeD are given in square brackets.

		$R(J'')$		$Q(J'')$		$P(J'')$	
Ω'–Ω''	J''	$f-f$	$e-e$	$e-f$	$f-e$	$f-f$	$e-e$
	7/2	22 309.8530	22 309.8530				
		[22 309.8688]	[22 309.8688]				
	9/2	22 319.2648	22 319.2648	22 282.8703	22 282.8703		
		[22 319.2967]	[22 319.2967]				
	11/2	22 329.2039	22 329.2039	22 286.1889	22 286.1889	22 249.7924	22 249.7924
9/2–7/2		[22 329.2521]	[22 329.2521]				
	13/2	22 339.6324	22 339.6324	22 289.9840	22 289.9840	22 246.9626	22 246.9626
		[22 339.7016]	[22 339.7016]				
	15/2	22 350.4718	22 350.4804	22 294.2026	22 294.2111	22 244.5682	
	17/2	22 361.7145	22 361.7311	22 298.8187	22 298.8353	22 242.4987	
	19/2	22 373.3048	22 373.3363	22 303.7625	22 303.7940		
	5/2	22 285.8651	22 285.8651				
	7/2	22 291.9618	22 291.9693	22 262.0148	22 262.0148		
7/2–5/2	9/2	22 297.9648	22 297.9893	22 261.3298	22 261.3537		
	11/2	22 303.9045	22 303.9664	22 260.5833	22 260.6441		

expected to change by very much from their counterparts in FeH, so the 0–0 bands of the g $^6\Phi$–a $^6\Delta$ and g $^6\Phi$–b $^6\Pi$ systems were readily identified. Isotopic scaling of vibrational frequencies between FeH and FeD facilitated assignment of the remaining features to the 0–1, 0–2 and 0–3 bands of the g $^6\Phi$–a $^6\Delta$ transition and to the 0–1 band of the g $^6\Phi$–b $^6\Pi$ transition. Thus, the dispersed fluorescence spectra allowed for the characterization of two new electronic states in a variety of vibrational levels.

Figure 6 shows the 0–0 band of the g $^6\Phi_{9/2}$–a $^6\Delta_{7/2}$ transition obtained by pumping the J = 9/2 and J = 11/2 levels of the g $^6\Phi_{9/2}$ state. Transitions arise both from the upper level directly pumped and from nearby rotational levels due to collisional transfer of population before the upper state decays. As was the case in the g $^6\Phi$–X $^4\Delta$ transition, the R branch is very strong, the Q branch moderate, and the P branch weak. The rotational assignments for this spectrum (and all others taken in dispersed fluorescence) were made with upper state combination differences for the g $^6\Phi$ state from Sec. III A.

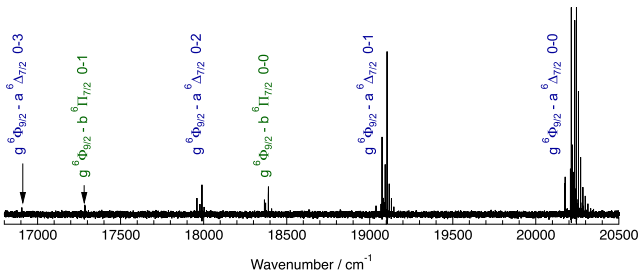

FIG. 5. An overview of the dispersed fluorescence spectrum obtained by pumping the *J* = 11/2 rotational level of the 0–0 g $^6\Phi_{9/2}$–X $^4\Delta_{7/2}$ band in FeD.

The 0–0 g $^6\Phi_{7/2}$–a $^6\Delta_{5/2}$ spectrum (Fig. 7) obtained by pumping the J = 11/2 level of the g $^6\Phi_{7/2}$ state reveals a more complex structure. In addition to the expected spectrum, the g $^6\Phi_{9/2}$–a $^6\Delta_{7/2}$ 0–0 band appears weakly, presumably due to collisional transfer from the g $^6\Phi_{7/2}$ state to the lower-lying g $^6\Phi_{9/2}$ state. (Previous studies of FeH referenced in the Introduction have established that electronic states in both the quartet and sextet manifolds have an inverted spin structure, with the substate of highest Ω lying lowest in energy.) In addition, a third band appears as strongly as does the main band, with the same upper state combination differences. This third feature was present in all dispersed fluorescence spectra from g $^6\Phi_{7/2}$ $v = 0$ regardless of which upper level was pumped; we will argue in Sec. V B that it arises from mixing between the a $^6\Delta_{5/2}$ $v = 0$ and A

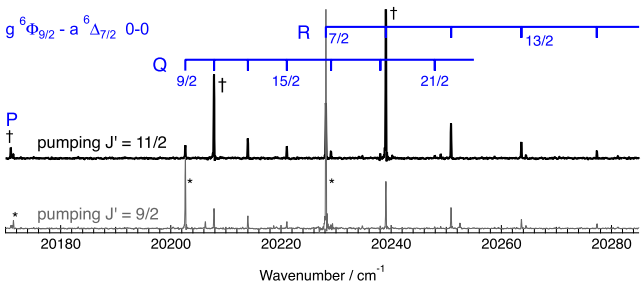

FIG. 6. The dispersed fluorescence spectrum of the 0–0 g $^6\Phi_{9/2}$–a $^6\Delta_{7/2}$ band of FeD, obtained by pumping the *J* = 9/2 level (lower trace, in gray) and the *J* = 11/2 level (upper trace, in black) of the g $^6\Phi$ state. Collisional relaxation distributes the population of the pumped levels to nearby rotational levels of the g $^6\Phi$ state. Transitions marked with an asterisk (*) or dagger (†) arise from the upper state level that has been directly pumped.

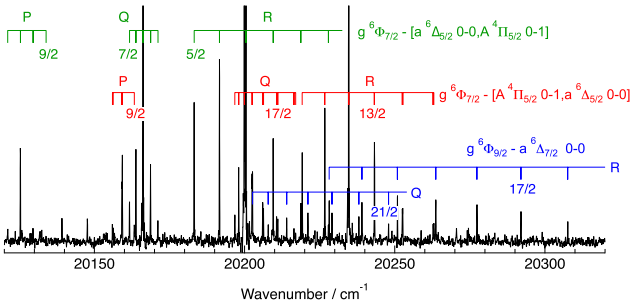

FIG. 7. The dispersed fluorescence spectrum obtained by pumping the $v = 0$, $J = 11/2$ level of the g $^6\Phi_{7/2}$ state. The lowest marked lines (blue) are from the 0–0 g $^6\Phi_{9/2}$–a $^6\Delta_{7/2}$ band of FeD and are due to collisional relaxation from the g $^6\Phi_{7/2}$ state to the g $^6\Phi_{9/2}$ state. The two higher sets of marked lines (red and green) arise from the $v = 0$ g $^6\Phi_{7/2}$ state and are transitions to the mixed $v = 0$ a $^6\Delta_{5/2}$ and $v = 1$ A $^4\Pi_{5/2}$ levels.

$^4\Pi_{5/2}$ $v = 1$ levels due to an accidental near-degeneracy particular to FeD.

Tables II and III list all of the transitions that were observed in dispersed fluorescence from the seven levels that were pumped. In some cases, the same transition could be measured several times with a variety of strengths in different spectra, in which case the average value is reported. As the table demonstrates, the dispersed fluorescence spectra provided a particularly rich source of new transitions in FeD. Lines measured in individual DF scans are given as data in the supplementary material.

C. The laser excitation and dispersed fluorescence spectra involving the g $^6\Phi_{11/2}$ state

The lowest-lying spin–orbit component of the g $^6\Phi$ state has $\Omega = 11/2$, but this state is inaccessible from X $^4\Delta$ due to the selection rule that $\Delta\Omega = 0, \pm 1$. We obtained information about the g $^6\Phi_{11/2}$ spin–orbit sublevel by acquiring a spectrum of the g $^6\Phi_{11/2}$–a $^6\Delta_{9/2}$ 0–1 band near 523 nm, which was more convenient to access with our lasers than the 0–0 band near 490 nm. A promising set of strong transitions was observed a few cm^{-1} higher than the transitions of the g $^6\Phi_{9/2}$–a $^6\Delta_{7/2}$ 0–1 band and dispersed fluorescence spectra from individual lines had the same qualitative appearance and structure as had been observed from the g $^6\Phi_{9/2}$ and g $^6\Phi_{7/2}$ states. The R branch was stronger than the Q branch and much stronger than the P branch, consistent with Brown's result for the analogous band in FeH[15] and our previous observations of FeD. In all, 23 lines of the g $^6\Phi_{11/2}$–a $^6\Delta_{9/2}$ 0–1 band were recorded in laser excitation. The dispersed fluorescence spectra included the 0–0, 0–1, and 0–2 bands of the g $^6\Phi_{11/2}$–a $^6\Delta_{9/2}$ system, but no transitions to the b $^6\Pi$ state were observed since its spin–orbit component of highest Ω has $\Omega = 7/2$, which is inaccessible in principle from a state with $\Omega = 11/2$. (Interestingly, lines of the g $^6\Phi_{11/2}$–b $^6\Pi_{7/2}$ 0–1 band of FeH have been reported.[20]) The lines measured in laser excitation are listed in Table IV and those measured in dispersed fluorescence (obtained by

TABLE II. Assigned lines of the g $^6\Phi$–a $^6\Delta$ transition of ^{56}FeD in cm^{-1}, measured in the RT source via dispersed fluorescence. Lines from the $\Omega' = 9/2$–$\Omega'' = 7/2$ and $\Omega' = 7/2$–$\Omega'' = 5/2$ subbands were obtained by exciting lines in the g $^6\Phi$–X $^4\Delta$ 0–0 transition (see Sec. III B), while those of the $\Omega' = 11/2$–$\Omega'' = 9/2$ subband were obtained from lines of the g $^6\Phi$–a $^6\Delta$ 0–1 transition (see Sec. III C). Lines marked with a star (*) were obtained in the laser excitation experiments described in Sec. III C. The absolute uncertainty in the measurements is estimated at 0.005–0.007 cm^{-1} for the stronger lines. Assignment of *e*/*f* labels assumes that the ordering of these levels in the a $^6\Delta$ and A $^4\Pi$ states for a given J are the same as in FeH. Lines assigned to the g $^6\Phi_{7/2}$–[a $^6\Delta_{5/2}$ 0–0,A $^4\Pi_{5/2}$ 0–1] transition are in normal font, while those of the g $^6\Phi_{7/2}$–[A $^4\Pi_{5/2}$ 0–1,a $^6\Delta_{5/2}$ 0–0] transition are given in italics (see Sec. V B for an explanation of the transition labels).

			$R(J'')$		$Q(J'')$		$P(J'')$	
Ω'–Ω''		J''	$f-f$	$e-e$	$e-f$	$f-e$	$f-f$	$e-e$
11/2–9/2	$v = 0$	9/2	20 234.7695	20 234.7695				
		11/2	20 248.9888	20 248.9888	20 204.3577	20 204.3577		
		13/2	20 264.4623	20 264.4623	20 213.0471	20 213.0471	20 168.4152	20 168.4152
		15/2	20 281.1547	20 281.1547	20 222.9836	20 222.9836		
		17/2	20 299.0143	20 299.0143			20 175.9816	20 175.9816
		19/2	20 318.0246	20 318.0246				
		21/2					20 188.3867	20 188.3867
	$v = 1$	9/2	19 101.6035	19 101.6035				
		11/2	19 115.9831	19 115.9831	19 071.3513	19 071.3513		
		13/2	19 131.6795	19 131.6795	19 080.2605	19 080.2605		
		15/2	19 148.6535	19 148.6535	19 090.4887	19 090.4887		
		17/2	19 166.8950	19 166.8950	19 102.0115	19 102.0115	19 043.8495	19 043.8495
		19/2			19 114.8213	19 114.8213		
		21/2					19 057.3193	19 057.3193
	$v = 2$	9/2	17 983.3927	17 983.3927				
		11/2			17 953.8619	17 953.8619		
		13/2	18 014.9456	18 014.9456				
		15/2			17 974.8041	17 974.8041		
		17/2	18 052.2539	18 052.2539				

TABLE II. (*Continued*.)

			$R(J'')$		$Q(J'')$		$P(J'')$	
Ω'–Ω''		J''	$f-f$	$e-e$	$e-f$	$f-e$	$f-f$	$e-e$
9/2–7/2	$v=0$	7/2	20 228.1431	20 228.1431				
		9/2	20 239.0279	20 239.0279	20 202.6301	20 202.6301		
		11/2	20 250.8601	20 250.8601	20 207.8375	20 207.8375	20 171.4214	20 171.4214
		13/2	20 263.6232	20 263.6232	20 213.9836	20 213.9836	20 170.9600	20 170.9600
		15/2	20 277.3303	20 277.3303	20 221.0573	20 221.0573	20 171.4214	20 171.4214
		17/2	20 291.9734	20 291.9734	20 229.0712	20 229.0712	20 172.8025	20 172.8025
		19/2	20 307.5561	20 307.5561	20 238.0179	20 238.0179	20 175.1194	20 175.1194
		21/2	20 324.0942	20 324.0942	20 247.9160	20 247.9160	20 178.3757	20 178.3757
		23/2	20 341.5470	20 341.5470	20 258.7565	20 258.7565	20 182.5598	20 182.5598
		25/2		20 270.5288	20 270.5288			
	$v=1$	7/2	19 087.4801	19 087.4801				
		9/2	19 098.9621	19 098.9621	19 062.5707	19 062.5707		
		11/2	19 111.5140	19 111.5140	19 068.4901	19 068.4901		
		13/2	19 125.0938	19 125.0938	19 075.4541	19 075.4541	19 032.4272	19 032.4272
		15/2	19 139.7110	19 139.7110	19 083.4374	19 083.4374	19 033.7975	19 033.7975
		17/2	19 155.1739	19 155.3947	19 092.2684	19 092.4816		
		19/2	19 172.0449	19 172.2449	19 102.5184	19 102.7103		
	$v=2$	7/2	17 972.4823	17 972.4823				
		9/2	17 984.3976	17 984.3976	17 948.0050	17 948.0050		
		11/2	17 997.5002	17 997.5002	17 954.4691	17 954.4691		
		13/2	18 011.7509	18 011.7509	17 962.1061	17 962.1061		
		15/2			17 970.9096	17 970.9096		
		17/2			17 980.8496	17 980.8496		
	$v=3$	7/2	16 887.7925	116 887.7925				
		9/2	16 900.1272	16 900.1272				
		11/2	16 913.7280	16 913.7280				
7/2–5/2	$v=0$	5/2	20 183.1811	20 183.1811				
			20 219.1584	*20 219.1584*				
		7/2	20 191.6156	20 191.6156	20 161.6631	20 161.6631		
			20 226.6757	*220 226.6757*	*20 196.7214*	*20 196.7214*		
		9/2	20 200.4274	20 200.4274	20 163.7935	20 163.7935	20 133.9031	20 133.9031
			20 234.6481	*20 234.6481*	*20 198.0102*	*20 198.0102*		
		11/2	20 209.4920	20 209.4920	20 166.1765	20 166.1765	20 129.5426	20 129.5426
			20 243.1821	*20 243.1821*	*20 199.8828*	*20 199.8828*	*20 163.2759*	*20 163.2759*
		13/2	20 218.6831	20 218.6831	20 168.6796	20 168.6796	20 125.3556	20 125.3556
			20 252.4908	*20 252.6274*	*20 202.4549*	*20 202.6108*	*20 159.1533*	*20 159.2936*
		15/2	20 227.8659	20 227.8659	20 171.1268	20 171.1268	20 121.0992	20 121.0992
			20 262.7331	*20 262.9815*	*20 206.0031*	*20 206.2576*	*20 155.9839*	*20 156.2170*
		17/2			*20 210.6362*	*20 211.0329*		
		19/2			*20 216.4182*	*20 216.9918*		
	$v=1$	5/2	19 058.8778	19 058.8778				
		7/2	19 068.5028	19 068.5028	19 038.5534	19 038.5534		
		9/2	19 079.0055	19 079.0055	19 042.3754	19 042.3754		
		11/2	19 090.3843	19 090.3843	19 047.0718	19 047.0718	19 010.4283	19 010.4283
		13/2	19 102.6713	19 102.6713	19 052.6648	19 052.6648	19 009.3389	19 009.3389
		15/2	19 115.7299*	19 115.8243*	19 059.0534	19 059.0534	19 008.9777	19 008.9777
	$v=2$	5/2	17 942.9499	17 942.9499				
		7/2	17 953.0750	17 953.0750	17 923.1477	17 923.1477		
		9/2	17 964.2348	17 964.2348	17 927.6038	17 927.6038		
		11/2	17 976.3662	17 976.3662	17 933.0564	17 933.0564		
		13/2		17 939.4546	17 939.4546	17 896.1584	17 896.1584	

TABLE III. Assigned lines of the g $^6\Phi$–b $^6\Pi$ transition of ^{56}FeD in cm^{-1}, measured in the RT source via dispersed fluorescence. The absolute uncertainty in the measurements is estimated at 0.007 cm^{-1} for the stronger lines. Assignment of *e*/*f* labels assumes that the ordering of these levels in the b $^6\Pi$ state for a given *J* are the same as in FeH.

			$R(J'')$		$Q(J'')$		$P(J'')$	
Ω'–Ω''		J''	$f-f$	$e-e$	$e-f$	$f-e$	$f-f$	$e-e$
9/2–7/2	$v=0$	7/2	18 367.4533	18 367.4533				
		9/2	18 384.5631	18 385.1422	18 348.1590	18 348.7329		
		11/2	18 403.6359	18 405.5783	18 360.6190	18 362.5735		
		13/2	18 424.2445	18 428.6634	18 374.6151	18 379.0222		
	$v=1$	7/2	17 262.0686	17 262.0686				
		9/2	17 279.6740	17 280.3323	17 243.2838	17 243.9205		
		11/2	17 299.3550	17 301.2504	17 256.3727	17 258.2773		
		13/2			17 270.6481	17 276.2367		
7/2–5/2	$v=0$	5/2	18 451.4288	18 453.4169				
		7/2	18 465.5873	18 473.1789	18 435.6636			
		9/2	18 480.0386	18 495.6178	18 443.4263	18 459.0005		
		11/2	18 494.5104	18 518.9633	18 451.1910	18 475.2868		

pumping the J' = 11/2, 15/2, and 19/2 levels of the g $^6\Phi_{11/2}$ v = 0 state) are given in Table II. The lines of the 0–1 band that are in common between Tables II and IV and are in good agreement.

D. Lifetime measurements

We have obtained lifetime measurements from a few different levels of FeH and FeD in the molecular jet source, in which the collision rate between particles is very low. The accessible levels were from the g $^6\Phi_{9/2}$ and g $^6\Phi_{7/2}$ states, which we could directly pump from the X $^4\Delta$ state. In principle, we could also obtain lifetimes from the g $^6\Phi_{11/2}$ state, which we can access from the a $^6\Delta$ state but not from the X $^4\Delta$ state, but in the jet source the signal was too weak to obtain reasonable results. We did not attempt lifetime measurements from the RT source, since the higher collision rate could affect the results. To check our procedure, we measured the lifetime of the z ^{5}D$^o_4$ level of atomic iron, which is the upper state of a transition at 526.954 nm. Our result of 92 ± 5 ns can be compared to previous measurements of 89 ± 5 ns made in 1974[30] and 78 ± 4 ns made in 1991.[31] Our value compares more favorably with the earlier measurement, which was made in an atomic beam with a density of about 10^{10} atoms/cm^3. The pressure of the source in which the later measurement was made was about 10^{-4} Torr, as compared to about 10^{-5} Torr in our cold-beam molecular jet source. We have assessed uncertainty in our measurements at about 5% of the lifetime value, consistent with the previously mentioned experiments and with the scatter observed in repeated measurements of decay from the same upper level in our data.

We measured lifetimes in FeH by exciting the J = 9/2 and 11/2 levels of the g $^6\Phi_{9/2}$ state via the g $^6\Phi_{9/2}$–X $^4\Delta_{7/2}$ R(7/2) and R(9/2) lines. Our values of 59 ± 3 and 64 ± 3 ns can be compared to Brown's value of 38 ns from the J = 9/2 level. The discrepancy might be due to collisions in Brown's source that would tend to reduce the apparent lifetime. We then measured lifetimes of the g $^6\Phi_{9/2}$, J = 9/2, 11/2 levels (83 ± 4 ns, 81 ± 4 ns) and of the g $^6\Phi_{7/2}$, J = 7/2, 9/2 levels (88 ± 4 ns, 80 ± 4 ns) in FeD. The lifetimes of g $^6\Phi$ state levels in FeD are longer than those of comparable levels in FeH by 30%–40%.

TABLE IV. Assigned lines of the g $^6\Phi_{11/2}$–a $^6\Delta_{9/2}$ 0–1 band of ^{56}FeD in cm^{-1}, measured in the RT source via laser excitation spectroscopy. The absolute uncertainty in the measurements is estimated at 0.004 cm^{-1}, about 1/10th of the Doppler-broadened linewidth. Parity doubling was not resolved in this spectrum.

J''	$R(J'')$	$Q(J'')$	$P(J'')$
9/2	19 101.6051		
11/2	19 115.9851	19 071.3530	
13/2	19 131.6762	19 080.2599	19 035.6283
15/2	19 148.6571	19 090.4888	19 039.0734
17/2	19 166.8940	19 102.0200	19 043.8523
19/2	19 186.3730	19 114.8210	19 049.9430
21/2	19 207.0440	19 128.8730	19 057.3150
23/2	19 228.8810	19 144.1270	19 065.9508
25/2		19 160.5550	19 075.7930

IV. ANALYSIS

A. Term values for levels of FeD

As a first step in our analysis, we generated term values for rotational levels of ^{56}FeD in various electronic and vibrational states from our line lists and from the data for X $^4\Delta$ given in Ref. 25. The observed electronic substates were grouped as follows (see Fig. 1):

- X $^4\Delta_{7/2}$–a $^6\Delta_{7/2}$–b $^6\Pi_{7/2}$–g $^6\Phi_{9/2}$
- X $^4\Delta_{5/2}$–a $^6\Delta_{5/2}$–A $^4\Pi_{5/2}$–b $^6\Pi_{5/2}$–g $^6\Phi_{7/2}$
- a $^6\Delta_{9/2}$–g $^6\Phi_{11/2}$.

A set of connected term values could be generated for each group, but the groups themselves could not be connected together since information on the spin–orbit separation within electronic states of FeD is not yet available. The lowest-lying rotational level within

each group was set to an energy of 0 cm^{-1}. Thus, the term energies for states in the first group are consistent with Brown's choice of zero energy, while those in the second group require addition of a constant value a corresponding to the X $^4\Delta_{7/2}$ (J = 7/2) –X $^4\Delta_{5/2}$ (J = 5/2) interval and those in the third group require a constant b corresponding to the X $^4\Delta_{7/2}$ (J = 7/2)–a $^6\Delta_{9/2}$ (J = 9/2) interval. In FeH a = 163.98 cm^{-1} and b = 1890.83 cm^{-1}, the FeD values will be quite similar to these. Note that with our choices of zero energy, the lowest rotationless term energy will be less than zero, since it lies below the lowest rotational level of a given group.

Dr. C. Western's PGOPHER program[32] was employed to generate term values from the observed transitions with the "energy override" option available at the manifold level of the program's hierarchy. Up to seven independent measurements of a given transition were obtained via laser excitation or dispersed fluorescence spectra. When multiple readings of a line were made, each was weighted with its estimated uncertainty, determined by the method of observation and the transition's relative strength. The complete list of term values generated is given as data in the supplementary material.

B. Fitting to obtain molecular parameters for FeD and FeH

Many papers from Brown's group demonstrate that the standard molecular Hamiltonian models do not work well to describe energy levels in FeH. Residuals from fitting to obtain molecular parameters from the data are many times the uncertainty in the measurements. While the parameters describing the grosser energy structure for a given state, like the term energy T and the rotational constant B, are reasonably accurate, parameters describing the finer structure must be considered effective and cannot be readily interpreted in terms of the detailed physical structure of FeH. Past attempts to fit all spin–orbit substates of a given electronic state with a single Hamiltonian have been unsuccessful (see, for example, Refs. 23 and 9 for the X $^4\Delta$ state). Our initial analyses showed that this situation persists for FeD. In view of this, we have chosen to fit the term values for a given spin–orbit substate independently. Although term-value fitting is in general not recommended,[33] the problems associated with the procedure are small compared to the complications associated with using a standard Hamiltonian for the fitting.

To facilitate fair comparison of fitting parameters between isotopologues, we have chosen to refit the FeH term values from Brown's work (or, for X $^4\Delta$, from Ref. 10) with the same choice of Hamiltonian as we used for FeD. The Hamiltonian used depended upon the electronic state under consideration. For levels of the g $^6\Phi$ and a $^6\Delta$ states, the fits were conducted in PGOPHER using only the relevant diagonal term of the full Hamiltonian matrix. In anticipation of performing isotopic comparisons, we used the R^2 form of the Hamiltonian rather than the more commonly used N^2 form, since it more cleanly separates the rotational contributions from the electronic-vibrational contributions to the energy of a state. (Even so, rotational terms of the form $B < L_x^2 + L_y^2 >$ remain embedded in the term energies T.) No significant Λ-doubling was observed in the g $^6\Phi$ and a $^6\Delta$ states of FeD, and the doubling in the same states in FeH was small (<0.2 cm^{-1}), so no Λ-doubling terms were used in the Hamiltonians for these states. The fitting therefore averaged over the parity components for a given value of J. The parameters obtained by the fitting are given in Tables V and VI. The rather large uncertainties in many of the parameters, and the large standard deviations of the fittings compared to the measurement uncertainties, reflect the deficiencies in modeling the energy structure of FeH and FeD with a standard molecular Hamiltonian. The frequent determination of negative (and therefore unphysical) distortion parameters D emphasizes the effective nature of the fitting.

TABLE V. Molecular parameters (in cm^{-1}) obtained from fitting the v = 0 levels of the lowest three spin–orbit substates of the g $^6\Phi$ state of FeD and corresponding states of FeH from the work of Brown's group. 1σ uncertainties in the last reported digits are given in parentheses. The ratio of rotational constants B in the two isotopologues is given in the last column. The constants a and b, described in the text, respectively refer to the unknown interval between the lowest two spin–orbit components of the X $^4\Delta$ state in FeD and the unknown separation between the lowest spin–orbit components of the X $^4\Delta$ and a $^6\Delta$ states.

Ω	v	Parameter	FeD	FeH	Ratio
11/2	0	T_0	20 207.273 4(14) + b	22 104.96(17)	
		B_0	3.439 271(58)	6.902 6(171)	0.498
		D_0	0.188 31(41) × 10^{-3}	4.181(394) × 10^{-3}	
		H_0		2.107(234) × 10^{-6}	
9/2	0	T_0	22 273.458 1(13)	22 241.796(76)	
		B_0	3.307 949(70)	6.356 33(340)	0.520
		D_0	−0.016 38(57) × 10^{-3}	−0.440 4(256) × 10^{-3}	
7/2	0	T_0	22 245.969(13) + a	22 361.312(51)	
		B_0	3.322 98(100)	6.327 78(420)	0.525
		D_0	−0.095(123) × 10^{-3}	−1.306 3(547) × 10^{-3}	

TABLE VI. Molecular parameters (in cm^{-1}) obtained from fitting various vibrational levels observed in the lowest three spin–orbit substates of the a $^6\Delta$ state of FeD and corresponding states of FeH from the work of Brown's group. 1σ uncertainties in the last reported digits are given in parentheses. The ratio of rotational constants B in the two isotopologues is given in the last column. See the caption of Table V for a description of the constants a and b.

Ω	v	Parameter	FeD	FeH	Ratio
9/2	0	T_0	$-19.370\,8(27) + b$	1855.625(50)	
		B_0	2.765 234(49)	5.025 09(306)	0.538
		D_0		$-0.304(29) \times 10^{-3}$	
	1	T_1	$1113.905\,7(27) + b$	3475.161(94)	
		B_1	2.751 867(136)	5.138 56(546)	0.536
		D_1	$0.073\,3(12) \times 10^{-3}$	$-1.966\,4(568) \times 10^{-3}$	
	2	T_2	$2232.523\,4(60) + b$	4899.92(12)	
		B_2	2.692 98(54)	5.589 42(835)	0.482
		D_2	$0.134\,1(76) \times 10^{-3}$	$4.812(141) \times 10^{-3}$	
		H_2		$11.633(637) \times 10^{-6}$	
7/2	0	T_0	2053.346 4(35)	2010.869(77)	
		B_0	2.834 44(14)	5.190 89(396)	0.546
		D_0	$-0.026\,59(92) \times 10^{-3}$	$-0.485\,0(335) \times 10^{-3}$	
	1	T_1	3194.724 7(90)	3574.14(17)	
		B_1	2.762 246(675)	5.500 3(168)	0.502
		D_1	$-0.132\,63(814) \times 10^{-3}$	$-2.169(250) \times 10^{-3}$	
	2	T_2	4310.151 0(73)	5115.501(129)	
		B_2	2.720 88(27)	5.100 7(108)	0.533
		D_2		$0.863(185) \times 10^{-3}$	
		H_2		$7.025(813) \times 10^{-6}$	
	3	T_3	5395.312(13)		
		B_3	2.674 14(46)		
5/2	0	T_0	$2069.244(44) + a$	2164.715(184)	
		B_0	3.022 98(292)	5.464 2(144)	0.553
		D_0	$-1.102\,3(315) \times 10^{-3}$	-0.794×10^{-3}	
	1	T_1	$3195.085\,0(504) + a$	3746.28(14)	
		B_1	2.900 31(345)	5.509 6(64)	0.526
		D_1	$-0.036\,2(382) \times 10^{-3}$		
	2	T_2	$4311.835(102) + a$	5280.637(283)	
		B_2	2.823 35(822)	4.781 7(232)	0.590
		D_2	$-0.138(101) \times 10^{-3}$	$-4.540(290) \times 10^{-3}$	

The Λ-doubling was stronger for the X $^4\Delta$ and A $^4\Pi$ states. To take this into account, analytic expressions for the diagonal terms of the relevant Hamiltonians were obtained from PGOPHER. The expressions for X $^4\Delta_{7/2}$ and X $^4\Delta_{5/2}$ did not contain explicit Λ-doubling terms, so we augmented them with expressions given by Brown[25] for the splitting in these states, which he generated via perturbation theory from the full Hamiltonian matrix. We performed an analysis of this type for A $^4\Pi_{5/2}$, which yielded the same result as for X $^4\Delta_{5/2}$. We programmed the augmented expressions into the Igor Pro package[34] and employed its internal fitting routines to generate the parameters given in Table VII.

A different approach to the fitting was adopted for the b $^6\Pi$ state data. As was the case in FeH, this state in FeD follows a Hund's case b coupling pattern and exhibits strong Λ-doubling. We followed Brown's fitting approach for this state[18,20] and averaged the energies of the e and f components for a given value of J. Like Brown, we fit

TABLE VII. Molecular parameters (in cm^{-1}) obtained from fitting various vibrational levels observed in the observed spin–orbit substates of the X $^4\Delta$, A $^4\Pi$, and b $^6\Pi$ states of FeD and (where applicable) corresponding states of FeH from the work of Brown's group. 1σ uncertainties in the last reported digits are given in parentheses. The ratio of rotational constants B in the two isotopologues is given in the last column. See the caption of Table V for a description of the constants a and b.

State	Ω	v	Parameter	FeD	FeH	Ratio
X $^4\Delta$		0	T_0	−14.957 823(65)	−25.929 335(74)	
			B_0	2.986 987(19)	5.151 793(22)	0.580
			D_0	$-0.511\,02(86)\times10^{-3}$	$-3.881\,0(10)\times10^{-3}$	
			H_0	$-0.997(10)\times10^{-6}$	$-12.815(10)\times10^{-6}$	
			$k_{7/2}$	$2.54(11)\times10^{-9}$	$72.843(40)\times10^{-9}$	
	7/2	1	T_1		1732.991 308(33)	
			B_1		5.114 698 0(79)	
			D_1		$-3.044\,04(23)\times10^{-3}$	
			H_1		$-8.334\,0(16)\times10^{-6}$	
			$k_{7/2}$		$38.236\,5(73)\times10^{-9}$	
		2	T_2		3425.17(11)	
			B_2		4.928 4(40)	
			D_2		$-2.730(31)\times10^{-3}$	
			$k_{7/2}$		$24.7(37)\times10^{-9}$	
	5/2	0	T_0	−20.472 62(15)+a	126.116 72(11)	
			B_0	3.415 178(21)	6.314 85(66)	0.541
			D_0	$-0.313\,45(44)\times10^{-3}$	$0.828\,4(19)\times10^{-3}$	
			$k_{5/2}$	$4.608\,5(98)\times10^{-6}$	$64.030\,2(43)\times10^{-6}$	
A $^4\Pi$	5/2	1	T_1	2053.849 3(38)+a		
			B_1	3.225 52(28)		
			D_1	$1.225\,6(39)\times10^{-3}$		
			$k_{5/2}$	$3.72(11)\times10^{-6}$		
b $^6\Pi$	7/2	0	T_0	3936.69(298)	3894.93(267)	
			B_0	3.854(247)	6.258 9(1935)	0.616
			D_0		$-5.28(260)\times10^{-3}$	
		1	T_1	5042.26(11)	5431.85(83)	
			B_1	3.744(244)	5.606(58)	0.668
			D_1		$-0.99(73)\times10^{-3}$	
	5/2	0	T_0	3827.58(42)+a	3940.63(35)	
			B_0	3.082(35)	5.628(56)	0.548
			D_0		$30.2(16)\times10^{-3}$	

a simple $T + B(N)\,(N+1) - D(N)^2(N+1)^2$ model to the averaged energies, with $N = 1$ assigned to the lowest term value. The results are given in Table VII. At this time, the data on the b $^6\Pi$ state are rather fragmentary, and a more robust analysis will likely have to wait until the allowed e $^6\Pi$–b $^6\Pi$ transition is observed and analyzed.

C. Vibrational analyses

The vibrational intervals deduced from the data in Tables VI and VII are given in Table VIII. There were enough data for the a $^6\Delta$ spin–orbit substates in FeD to extract values for T_e (the purely electronic energy) and the vibrational ω_e and $\omega_e x_e$ used in the standard expression for the vibrational energy of level v, with $G(v) = T_e + \omega_e(v+1/2) - \omega_e x_e(v+1/2)^2$, with the caveat that the uncertainties in the parameters were not defined when the number of parameters was equal to the number of measurements. A similar analysis was done for FeH, except for the a $^6\Delta_{9/2}$ substate, which experiences known vibrational perturbations to levels $v = 1$ and 2.[20]

TABLE VIII. The results (in cm^{-1}) of analysis of the vibrational structure of various spin–orbit substates of the X $^4\Delta$, a $^6\Delta$, and b $^6\Pi$ states in FeD and in the corresponding states of FeH. The intervals $\Delta G_{1/2,3/2,5/2}$ report the separation of the 1–0, 2–1, and 3–2 vibrational levels, while the parameters T_e, ω_e, and $\omega_e x_e$ are those defined in Sec. IV C. The ratio of selected analogous parameters in FeD and FeH is given in the last column Entries marked with an asterisk arise from vibrational levels that are known to be perturbed.

State		FeD	FeH	Ratio
X $^4\Delta_{7/2}$	$\Delta G_{1/2}$		1758.92	
a $^6\Delta_{9/2}$	$\Delta G_{1/2}$	1133.28	1619.54*	0.699
	$\Delta G_{3/2}$	1118.62	1424.75*	0.787
	T_e	$-591.51 + b$	1127.01	
	ω_e	1147.93	1522.15	0.758
	$\omega_e x_e$	7.329	0	
a $^6\Delta_{7/2}$	$\Delta G_{1/2}$	1141.38	1563.27	0.730
	$\Delta G_{3/2}$	1115.42	1541.36	0.725
	$\Delta G_{5/2}$	1085.16		
	T_e	1471.47(165)	1221.02	
	ω_e	1170.35(200)	1585.18	0.741
	$\omega_e x_e$	14.05(48)	10.96	
a $^6\Delta_{5/2}$	$\Delta G_{1/2}$	1125.84	1581.57	0.709
	$\Delta G_{3/2}$	1116.75	1534.35	0.730
	T_e	$1502.91+a$	1356.23	0.699
	ω_e	1134.93	1628.77	
	$\omega_e x_e$	4.55	23.60	
b $^6\Pi_{7/2}$	$\Delta G_{1/2}$	1105.57	1536.92	0.719

V. DISCUSSION

A. Comparisons of parameters between FeD, FeH, and theory

Our data on FeD invite comparison with previous measurements and theoretical calculations on FeH. We require the parameter $\rho = \sqrt{\mu_{(^{56}\mathrm{FeH})}/\mu_{(^{56}\mathrm{FeD})}}$ as defined in Ref. 35, where μ is the reduced mass of an isotopologue, to scale parameters of FeH in order to compare them with those for FeD. This ratio evaluates to 0.714 and its square to 0.509. The ratio of rotational parameters B is expected to scale as ρ^2, while the vibrational frequencies ω_e are expected scale as ρ, as are vibrational intervals ΔG to first order. However, these expectations must be tempered, since the large change in reduced mass (and therefore B) between FeD and FeH significantly affects the strength of rotational couplings between states. Such couplings arise from terms in the rotational Hamiltonian like $B\hat{J}_{\pm}\hat{L}_{\mp}$, which mixes electronic states, and $B\hat{J}_{\pm}\hat{S}_{\mp}$, which mixes spin–orbit sublevels within an electronic state. These effects are nearly twice as large in FeH as they are in FeD, so rotationally induced perturbations resulting from them will be stronger in FeH. Furthermore, the vibrational structure of each electronic state is greatly altered between the isotopologues, since the spacing of vibrational levels in FeD is about 7/10 of the spacing of levels in FeH. Thus, vibrational levels of different electronic states will change their relative position, which will increase their mutual interaction if they move closer together in one isotopologue relative to the other or decrease it if they move farther apart.

Tables V–VII show that the electronic energies of the g $^6\Phi$, a $^6\Delta$, and b $^6\Pi$ states FeH and FeD are quite close for the $v = 0$ levels of each spin–orbit component, as we expect. The ratio of rotational constants $B_{\mathrm{FeD}}/B_{\mathrm{FeH}}$ scatter rather widely around the nominal value of 0.509, particularly for the b $^6\Pi$ state, emphasizing the effective nature of the fittings as discussed in Sec. IV B. The values for the centrifugal distortion parameters D and Λ-doubling parameters k are typically more than an order of magnitude smaller in FeD as compared to FeH. In a highly effective fitting, these parameters compensate for some of the effects of rotational perturbations, and their smaller value in FeD reflects in part the reduced rotational couplings in this isotopologue. The scaling of vibrational intervals ΔG and equilibrium vibrational frequencies ω_e conforms reasonably well to the expected value of 0.714 for levels that are not perturbed.

B. Assignment of the A $^4\Pi_{5/2}$ $v = 1$ level

The spectrum shown in Fig. 7 includes three bands of which two share upper state rotational levels from the g $^6\Phi_{7/2}$ $v = 0$ state. The two spectra are of similar appearance and intensity, and they are shifted relative to one another by 30–40 cm^{-1}. Rotational analysis reveals that $\Omega = 5/2$ in each of the lower states, which lie about 2220–2240 cm^{-1} above the lowest rotational level of X $^4\Delta$, once the ~164 cm^{-1} spin–orbit separation of the X $^4\Delta_{7/2}$–X $^4\Delta_{5/2}$ states is added into the T values given in Tables VI and VII. We postulate that one of the bands is primarily the allowed g $^6\Phi_{7/2}$–a $^6\Delta_{5/2}$ 0–0 band expected in this region and that the lower state of the other band is another $\Omega = 5/2$ state heavily mixed with a $^6\Delta_{5/2}$ due to an accidental near-degeneracy. Thus, the unexpected band borrows intensity from the g $^6\Phi_{7/2}$–a $^6\Delta_{5/2}$ 0–0 band due to the a $^6\Delta_{5/2}$ character mixed into its lower state.

The only electronic states other than a $^6\Delta$ that lie below 2240 cm^{-1} are X $^4\Delta$ and A $^4\Pi$, each of which contains an $\Omega = 5/2$ spin–orbit substate. The vibrational structure of these states is not known from experiment in FeD, but we can estimate their values of ω_e by scaling the equilibrium vibrational frequencies reported in high-quality calculations of the lowest four electronic states of FeH.[12] The results are 0.714(1826.86 cm^{-1}) = 1304.4 cm^{-1} for X $^4\Delta$ and 0.714(1837.1 cm^{-1}) = 1311.7 cm^{-1} for A $^4\Pi$. These values place excited vibrational states of X $^4\Delta$ at about 1470 cm^{-1} ($v = 1$) and 2770 cm^{-1} ($v = 2$), once the ~164 cm^{-1} shift is added in. The A $^4\Pi_{5/2}$ $v = 0$ level lies at about 970 cm^{-1};[22] therefore, the $v = 1$ level position is about 2280 cm^{-1}. Note that the vibrational level estimates are likely slightly too high since the $\omega_e x_e$ parameters have not been taken into account in either electronic state.

Clearly, the A $^4\Pi_{5/2}$ $v = 1$ level is the best choice for the second $\Omega = 5/2$ lower state for the spectra shown in Fig. 7. Transitions from g $^6\Phi_{7/2}$ to this level are forbidden since $\Delta\Lambda = 2$, but the a $^6\Delta_{5/2}$ character imbued by mixing permits them to occur. The near-equal intensity of the two bands implies that the composition of both lower states is nearly a 50%/50% mixture of a $^6\Delta_{5/2}v = 0$ and A $^4\Pi_{5/2}v = 1$. As to which of the two bands has a dominantly a $^6\Delta_{5/2}$ lower-state structure and which has a A $^4\Pi_{5/2}$ structure, we see that the rotational parameter of the band at lower wavenumber (3.023 cm^{-1}; see Table VI) is a close match to other rotational parameters of the a $^6\Delta$ electronic state, while the higher-lying band has a larger constant of

3.226 cm^{-1} (Table VII). The calculated rotational parameters from Ref. 12 are higher for A $^4\Pi$ than they are for a $^6\Delta$. Furthermore, no Λ-doubling was observed in the a $^6\Delta$ states of FeD or in the lower state of the lower-lying band, while the lower state of the higher-lying band exhibits pronounced Λ-doubling, as is often the case in Π electronic states. We therefore assign the lower-lying band to g $^6\Phi_{7/2}$–[a $^6\Delta_{5/2}$ 0–0, A $^4\Pi_{5/2}$ 0–1] and the higher-lying band to g $^6\Phi_{7/2}$–[A $^4\Pi_{5/2}$ 0–1,a $^6\Delta_{5/2}$ 0–0], where the first label given for the lower state identifies its primary character.

We note that the g $^6\Phi$–b $^6\Pi$ transitions we have observed are also forbidden since $\Delta\Lambda = 2$. This implies that the b $^6\Pi$ states are also of mixed character, likely again due to their proximity to levels of the a $^6\Delta$ electronic state. Some analogous transitions were also observed in FeH.[20]

C. Analysis of ^{54}FeD and ^{54}FeH transitions and the vibrational frequency of the g $^6\Phi$ state

The switch of isotopologues between ^{56}FeD and ^{54}FeD (or between ^{56}FeH and ^{54}FeH) changes the molecule's energy structure by a small amount compared to the change introduced by deuterating FeH. The scaling factor $\rho = \sqrt{\mu_{(^{56}\mathrm{FeD})}/\mu_{(^{54}\mathrm{FeD})}}$, which scales ^{56}FeD parameters to those of ^{54}FeD, is 1.000 643, while for FeH it is 1.000 327. Brown's group observed ^{54}FeH transitions in the g $^6\Phi_{11/2}$–a $^6\Delta_{9/2}$ and g $^6\Phi_{9/2}$–a $^6\Delta_{7/2}$ spectra of FeH and used them to estimate the vibrational frequency of the g $^6\Phi$ state, but their results were affected by vibrational perturbations in the a $^6\Delta_{9/2}$ state[20] and by some contamination of the term energies T by rotational contributions. Their value[15] of 1440 ± 50 cm^{-1} as compared to the theoretical value[11] of 1773 cm^{-1} surprised them, and so a reconsideration of the g $^6\Phi$ state vibrational frequency is in order.

We have observed ^{54}FeD transitions in the R branch of the g $^6\Phi_{9/2}$–X $^4\Delta_{7/2}$ 0–0 band (see Table I), which are shifted a little to higher frequencies (0.015–0.070 cm^{-1}) compared to their ^{56}FeD counterparts. These small shifts were discernible since the data were taken in the molecular jet source, in which transitions have very small Doppler widths (~0.007 cm^{-1}) compared to those from the RT source (~0.040 cm^{-1}); indeed, Brown does not observe similar shifts in the FeH g $^6\Phi$–X $^4\Delta$ spectrum due to the breadth of his lines. We have scanned select R branch lines of the g $^6\Phi_{9/2}$–X $^4\Delta_{7/2}$ 0–0 band of FeH in the molecular jet and have recorded some ^{54}FeH transitions. We can therefore estimate the vibrational frequency of the g $^6\Phi$ state from both FeH and FeD isotopic data.

To minimize the rotational contributions to our analysis, we shall use only the R(7/2) line in the bands of interest, since it includes the lowest-lying rotational level in both the g $^6\Phi_{9/2}$ and X $^4\Delta_{7/2}$ spin–orbit substates. (Higher rotational excitations will include more contributions from the effective distortion constants D, which will not scale cleanly as ρ^4 because they include effects of perturbative interactions as well as standard distortion.) We can write the ρ-scaled wavenumber of an R line in this band as

$$R(J'') = T_{00}(\rho) + \rho^2\left(B_g\left[(J''+1)(J''+2) - \frac{55}{4}\right] - B_X\left[(J'')(J''+1) - \frac{43}{4}\right]\right), \quad (1)$$

$$T_{00}(\rho) = T_e + \frac{1}{2}\rho[(\omega_e)_g - (\omega_e)_X] + \rho^2\left[B_g < L_x^2 + L_y^2 >_g - B_X < L_x^2 + L_y^2 >_X\right]. \quad (2)$$

The R^2 rotational matrix elements in Eq. (1) were taken from PGOPHER. T_{00} is the difference of term energies between the $v = 0$ levels of the g $^6\Phi_{9/2}$ and X $^4\Delta_{7/2}$ states, which includes the purely electronic energy, the vibrational contribution (zero-point energy in this case)—which scales as ρ, and the rotational contribution—which scales as ρ^2 and cannot be included in the rotational matrix elements. When $\rho = 1$, we obtain the $R(J'')$ transition for the isotopologues containing ^{56}Fe.

We can use the measured R(7/2) transitions (22 311.8209 cm^{-1} in ^{56}FeH, 22 311.8389 in ^{54}FeH) and rotational constants from Tables V and VII to evaluate $T_{00}(\rho)$ for ^{56}FeH (23 267.6606 cm^{-1}) and ^{54}FeH (23 267.6497 cm^{-1}). Assuming that this rotational contribution in Eq. (2) is negligible, the difference 0.0109 cm^{-1} between the T_{00} for the ^{56}FeH isotopologue and the ^{54}FeH isotopologue is $\frac{1}{2}(1-\rho)[(\omega_e)_g - (\omega_e)_X]$. Thus, $(\omega_e)_g - (\omega_e)_X = -66.8$ cm^{-1}, and by setting $(\omega_e)_X$ to 1826.86 cm^{-1} as was done in Sec. V B, we obtain our estimate $(\omega_e)_g = 1760$ cm^{-1} for the vibrational frequency of the g $^6\Phi$ state. This result is in much closer agreement with the theoretical value of 1773 cm^{-1} than the estimate obtained by Brown.

The analysis can be repeated with isotopologues of FeD, yielding

$$^{56}\mathrm{FeD}: \quad T_{00} = 22\,288.4005 \text{ cm}^{-1}$$
$$^{54}\mathrm{FeD}: \quad T_{00} = 22\,288.3887 \text{ cm}^{-1}$$
$$\Delta T_{00} = 0.0118 \text{ cm}^{-1}$$
$$(\omega_e)_g - (\omega_e)_X = -36.7 \text{ cm}^{-1}.$$

The vibrational frequency of X $^4\Delta$ has not been measured in FeD; however, if we scale the FeH value by 0.714 (see Sec. V A) we obtain $(\omega_e)_X = 1303$ cm^{-1}, which yields $(\omega_e)_g = 1267$ cm^{-1}. The ratio of $(\omega_e)_g$ values between FeD and FeH then comes to 0.720, which demonstrates self-consistency between our FeH and FeD results.

VI. CONCLUSIONS

The results presented here greatly expand the available data on the FeD molecule, for which only data on the F $^4\Delta$ and X $^4\Delta$ states were previously available. The electronic states g $^6\Phi$, a $^6\Delta$, and b $^6\Pi$ have been observed for the first time, and their similarity and differences with FeH have been explored. Analysis reveals that while couplings between various electronic states are strongly evident in FeD, they are less severe than those of FeH. Thus, theoretical modeling of FeD may prove less difficult than is the case for FeH. Given the strong shifts in vibrational level positions between FeH and FeD, the combination of data from the two molecules will more completely sample the potential surfaces for the various electronic states studied so far, which will also improve efforts to model this molecule in both isotopic forms.

FeH is ubiquitous in stellar atmospheres of cooler M-class stars, and its spectrum can be used to measure the star's rotation rate and the strength of its magnetic field[36–38] and even to search for exoplanets orbiting the star.[39,40] Further studies of FeD add the possibility

of measuring the abundance of deuterium relative to hydrogen in M-class stars. We plan to next explore the rich variety of transitions accessible from the e $^6\Pi$ state of FeD, in analogy to a similar study by Brown's group on FeH.[16,19,21] We will also search for new states not yet observed in either FeH or FeD to build a more complete picture of this molecule. The Zeeman splitting of selected spectra of these molecules will be obtained as well to aid in the measurement of stellar magnetic fields.

SUPPLEMENTARY MATERIAL

The supplementary material includes a list of term values generated from the fitting presented in Sec. IV A and a listing of the transitions observed in all ten dispersed fluorescence spectra taken for this study.

ACKNOWLEDGMENTS

We are grateful to the Natural Sciences and Engineering Research Council of Canada for financial support through Discovery grants (DWT, AGA) and an Undergraduate Student Research Award (RARH). We thank Joyce MacGregor for maintaining and running our ring laser and Dr. Colan Linton for helpful discussions and advice.

AUTHOR DECLARATIONS

Conflict of Interest

The authors have no conflicts to disclose.

Author Contributions

R. A. R. Harvey: Formal analysis (equal); Investigation (equal); Methodology (equal); Writing – review & editing (equal). **D. W. Tokaryk**: Conceptualization (equal); Data curation (lead); Formal analysis (equal); Investigation (equal); Methodology (equal); Supervision (equal); Writing – original draft (lead). **A. G. Adam**: Conceptualization (equal); Investigation (equal); Methodology (equal); Supervision (equal); Writing – review & editing (equal).

DATA AVAILABILITY

The raw data files for both the laser excitation spectra and the dispersed fluorescence spectra collected via Fourier transform spectroscopy are available from the authors upon request.

REFERENCES

[1] P. K. Carroll and P. McCormack, "The spectrum of FeH: Laboratory and solar identification," Astrophys. J. Lett. **177**, 33 (1972).
[2] H. L. Nordh, B. Lindgren, and R. F. Wing, "A proposed identification of FeH in the spectra of M dwarfs and S stars," Astron. Astrophys. **56**, 1–6 (1977).
[3] R. E. S. Clegg and D. L. Lambert, "On the identification of FeH and CeO in S stars," Astrophys. J. **226**, 931–936 (1978).
[4] R. P. Schiavon, B. Barbuy, and P. D. Singh, "The FeH Wing–Ford band in the spectra of M stars," Astrophys. J. **484**, 499–510 (1997).
[5] J. J. Harrison, J. M. Brown, J. Chen, T. C. Steimle, and T. J. Sears, "The Zeeman effect on lines in the (1,0) band of the $F^4\Delta$-$X^4\Delta$ transition of the FeH radical," Astrophys. J. **679**, 854 (2008).
[6] P. Crozet, G. Dobrev, C. Richard, and A. J. Ross, "Determination of Landé factors in the F $^4\Delta_{5/2,7/2}$ state of ^{56}FeH by laser excitation spectroscopy," J. Mol. Spectrosc. **303**, 46–53 (2014).
[7] P. K. Carroll, P. McCormack, and S. Oconnor, "Iron hydride: Laboratory studies and solar identification," Astrophys. J. **208**, 903–913 (1976).
[8] W. J. Balfour, B. Lindgren, and S. O'Connor, "On the 1μm system of iron hydride," Chem. Phys. Lett. **96**, 251–252 (1983).
[9] W. J. Balfour, "Rotational analysis of the 9877 and 8960 Å bands of FeD," Phys. Scripta **28**, 551–560 (1983).
[10] J. G. Phillips, S. P. Davis, B. Lindgren, and W. J. Balfour, "The near-infrared spectrum of the FeH molecule," Astrophys. J., Suppl. Ser. **65**, 721–778 (1987).
[11] S. R. Langhoff and C. W. Bauschlicher, Jr., "Theoretical study of the spectroscopy of FeH," J. Mol. Spectrosc. **141**, 243–257 (1990).
[12] N. J. DeYonker and W. D. Allen, "Taming the low-lying electronic states of FeH," J. Chem. Phys. **137**, 234303 (2012).
[13] D. A. Fletcher, R. T. Carter, J. M. Brown, and T. C. Steimle, "The green system of FeH recorded at ambient temperatures," J. Chem. Phys. **93**, 9192–9193 (1990).
[14] R. T. Carter, T. C. Steimle, and J. M. Brown, "The identification of a $^6\Phi$-$X^4\Delta$ intercombination system in the FeH radical at 448 nm," J. Chem. Phys. **99**, 3166–3173 (1993).
[15] R. T. Carter and J. M. Brown, "Observation and identification of the g $^6\Phi$-a $^6\Delta$ transition in the blue system of FeH at 493 nm," J. Chem. Phys. **101**, 2699–2709 (1994).
[16] D. M. Goodridge, R. T. Carter, J. M. Brown, and T. C. Steimle, "Rotational analysis and assignment of the green band system of FeH to the e $^6\Pi$-a $^6\Delta$ transition," J. Chem. Phys. **106**, 4823–4831 (1997).
[17] D. F. Hullah, C. Wilson, R. F. Barrow, and J. M. Brown, "New assignments in the green and red band systems of the FeH radical," J. Mol. Spectrosc. **192**, 191–197 (1998).
[18] D. F. Hullah, R. F. Barrow, and J. M. Brown, "Low-lying energy levels of the FeH molecule," Mol. Phys. **97**, 93–103 (1999).
[19] C. Wilson and J. M. Brown, "Identification of new hot bands in the blue and green band systems of FeH," J. Mol. Spectrosc. **197**, 188–198 (1999).
[20] C. Wilson and J. M. Brown, "The FeH radical: Rotational assignment of the a $^6\Delta$ (v=2) and b $^6\Pi$ (v=1) levels," Mol. Phys. **99**, 1549–1561 (2001).
[21] C. Wilson and J. M. Brown, "Evidence for a strong intercombination transition in FeH at around 510 nm," J. Mol. Spectrosc. **209**, 192–197 (2001).
[22] W. J. Balfour, J. M. Brown, and L. Wallace, "Electronic spectra of iron monohydride in the infrared near 1.35 and 1.58 μm," J. Chem. Phys. **121**, 7735–7742 (2004).
[23] J. M. Brown, H. Körsgen, S. P. Beaton, and K. M. Evenson, "The rotational and fine-structure spectrum of FeH, studied by far-infrared laser magnetic resonance," J. Chem. Phys. **124**, 234309 (2006).
[24] G. V. Chertihin and L. Andrews, "Infrared spectra of FeH, FeH_2, and FeH_3 in solid argon," J. Phys. Chem. **99**, 12131–12134 (1995).
[25] M. Jackson, L. R. Zink, J. P. Towle, N. Riley, and J. M. Brown, "The rotational spectrum of the FeD radical in its X $^4\Delta$ state, measured by far-infrared laser magnetic resonance," J. Chem. Phys. **130**, 154311 (2009).
[26] S. P. Beaton, K. M. Evenson, T. Nelis, and J. M. Brown, "Detection of the free radicals FeH, CoH, and NiH by far infrared laser magnetic resonance," J. Chem. Phys. **89**, 4446–4448 (1988).
[27] A. G. Adam, L. P. Fraser, W. D. Hamilton, and M. C. Steeves, "Gas-phase electronic spectroscopy of cobalt monofluoride," Chem. Phys. Lett. **230**, 82–86 (1994).
[28] B. G. Guislain, R. A. R. Harvey, D. W. Tokaryk, A. J. Ross, P. Crozet, and A. G. Adam, "An alternative approach to interferogram collection and processing for a vintage Bomem DA3 Fourier transform spectrometer," J. Mol. Spectrosc. **364**, 111181 (2019).
[29] H. M. Crosswhite, "The iron-neon hollow cathode spectrum," J. Res. Natl. Bur. Stand. **79A**, 17–53 (1975).
[30] H. Figger, K. Siomos, and H. Walther, "Lifetime measurements in the Fe I spectrum using tunable dye laser excitation," Z. Phys. **270**, 371–376 (1974).
[31] T. R. O'Brian, M. E. Wickliffe, J. E. Lawler, W. Whaling, and J. W. Brault, "Lifetimes, transition probabilities, and level energies in Fe I," J. Opt. Soc. Am. B **8**, 1185–1201 (1991).

[32]C. M. Western, "PGOPHER, a program for simulating rotational, vibrational and electronic spectra," J. Quant. Spectrosc. Radiat. Transfer **186**, 221–242 (2017).
[33]D. L. Albritton, W. J. Harrop, and A. L. Schmeltekopf, "A critique of the term value approach to determining molecular constants from the spectra of diatomic molecules," J. Mol. Spectrosc. **46**, 67–88 (1973).
[34]Wavemetrics, "Igor Pro from Wavemetrics | Igor Pro by Wavemetrics," https://www.wavemetrics.com (2022), accessed: 21 August 2022.
[35]G. Herzberg, *Molecular Spectra and Molecular Structure I. Spectra of Diatomic Molecules*, 2nd ed. (Van Nostrand Reinhold Company, New York, 1950).
[36]A. Reiners and G. Basri, "Measuring magnetic fields in ultracool stars and brown dwarfs," Astrophys. J. **644**, 497–509 (2006).
[37]A. Reiners and G. Basri, "The first direct measurements of surface magnetic fields on very low mass stars," Astrophys. J. **656**, 1121–1135 (2007).
[38]M. K. Browning, G. Basri, G. W. Marcy, A. A. West, and J. Zhang, "Rotation and magnetic activity in a sample of M-dwarfs," Astron. J. **139**, 504–518 (2010).
[39]C. Moutou, S. Dalal, J.-F. Donati, E. Martioli, C. P. Folsom, É. Artigau, I. Boisse, F. Bouchy, A. Carmona, N. J. Cook, X. Delfosse, R. Doyon, P. Fouqué, G. Gaisné, G. Hébrard, M. Hobson, B. Klein, A. Lecavelier des Etangs, and J. Morin, "Early science with SPIRou: Near-infrared radial velocity and spectropolarimetry of the planet-hosting star HD 189733," Astron. Astrophys. **642**, A72 (2020).
[40]A. Y. Kesseli, I. A. G. Snellen, F. J. Alonso-Floriano, P. Mollière, and D. B. Serindag, "A search for FeH in hot-Jupiter atmospheres with high-dispersion spectroscopy," Astron. J. **160**, 228 (2020).